Physical and Chemical Response of $FeCl_3/FeCl_4^-$ Spin Probes on the Functionalizing of Ionic Liquids

ARTICLE *in* THE JOURNAL OF PHYSICAL CHEMISTRY A · APRIL 2013

Impact Factor: 2.69 · DOI: 10.1021/jp403260r · Source: PubMed

2 AUTHORS, INCLUDING:

Werner Herrmann

Freie Universität Berlin

26 PUBLICATIONS **370** CITATIONS

THE JOURNAL OF PHYSICAL CHEMISTRY A

Article

pubs.acs.org/JPCA

Physical and Chemical Response of $FeCl_3/FeCl_4^-$ Spin Probes on the Functionalizing of Ionic Liquids

Reinhard Stößer[†] and Werner Herrmann*[,‡]

[†]Institut für Chemie, Humboldt-Universität zu Berlin, Brook-Taylor-Str. 2, D-12489 Berlin, Germany

[‡]Institut für Pharmazie, Freie Universität Berlin, Kelchstraße 31, D-12169 Berlin, Germany

ABSTRACT: Fe(III) compounds $FeCl_3$ and $FeCl_4^-$ have been used as ESR spin probes in ionic liquids (ILs) at 293 and 77 K for the first time. They showed characteristic spectral patterns, which could be separated from each other by simulation. The largest contribution originates from aggregated $FeCl_4^-$ and other exchange coupled species at $g' \approx 2.6$. $FeCl_4^-$ has been shown to be an identifiable, changeable, customizable, transferable, and extractable probe with contributions to a characteristic ESR fine structure. For simulation a spin Hamiltonian with up to fourth order and statistic distributions of spin coupling parameters has been used. The different Fe(III) signals coexist being dependent on the functionalization of the IL, i.e., on changing the chain length of the substituent at the imidazolium cation as well as varying the respective anion (BF_4^-, PF_6^-, Cl^-, and $FeCl_4^-$). From the molecular structure and occurrence of the Fe(III) species conclusions could be drawn concerning their locations and reactions in polar and nonpolar compartments of the ILs. Their contributions could be purposefully adjusted via the molecular control of the properties of the ILs. The conversion of $FeCl_3$ into $FeCl_4^-$ and $[FeCl_4X_2]^{3-}$ species could be observed to be dependent on the formation of polar and nonpolar domains in ILs.

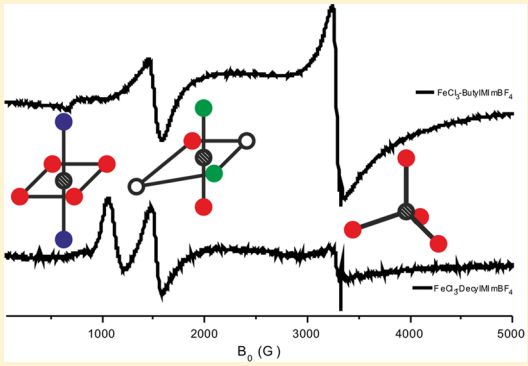

INTRODUCTION

For the past few years the complex properties of ionic liquids (ILs) have been the subject of many examinations already.[1−9] They are present in all fields of physical chemistry. They even offer new possibilities for carrying out physical and chemical examinations in condensed matter, fluid, and frozen phases, leading to new knowledge about respective internal properties.[10−15] Open questions are mainly concerned with details of the properties of ILs and their influence on the specific interactions with the solute on a molecular level, in particular with the formation of heterogeneous, e.g., secondary structures like domains and others.

As recent publications concerning the usage of spin probes indicate[16−19] within the manifold of examination methods electron spin resonance (ESR) spectroscopy is suitable to supply data for structure and dynamics of the systems. Up to now this is mainly related to spin probes characterized by $S = 1/2$. Moreover, there is some literature about other nonspin probes depending on physical and chemical properties of transition metals in ILs.[20−29]

As far as we know the higher information content of transition metal probes with $S > 1/2$ has not been used in this connection up to now. In particular, the possibilities of changing the state of oxidation and the change of ligands in such systems is challenging and might supply data which leads to an increase in the of understanding and applications of ILs.

The point of origin of the present paper is the question, which information can be delivered by ESR spectroscopy via Fe^{3+} ions ($I = 5/2$) about the complex structure of ILs (including the frozen solutions). For that purpose it had to be found out how the Fe^{3+} ion could be introduced to act as a spin probe. First experiments using Fe^{3+} halides (F^-, Cl^-, and Br^-[30−39]) in conventional solvents as well as in ILs led to the conviction that the species $FeCl_3$ or $FeCl_4^-$ might have a good chance to answer the questions raised above; that is, the iron species do not act only as reporters about the structure but also they can actively take part in the changes of the structure and report about it by changing their spectroscopic properties. This is particularly true for the formation of new binding interactions induced by components of the ILs or other added substances like Cl^-. The different kinds to introduce the anion $FeCl_4^-$ (e.g., as $HFeCl_4$, $ImFeCl_4$, and $KFeCl_4$) into the Fe^{3+}/IL system will be helpful for the signal assignment.

X-band ESR spectroscopy at room temperature and 77 K and a "model kit" for the complete simulation of the ESR spectra have been selected to be the means for the investigations, due to a lot of experience in that field.[40,41]

The aims of the investigations presented here are as follows:

- Recording the ESR spectra, complete quantitative spectra analysis, and assignment of the observed transitions using a "model kit" and considering the statistical distributions[42] of the zero field splitting (zfs) parameters.

Received: April 2, 2013
Revised: April 13, 2013
Published: April 18, 2013

   dx.doi.org/10.1021/jp403260r | J. Phys. Chem. A 2013, 117, 3960−3971

- Assignment of the individual spectral contributions of the experimental spectra to chemical species (see, e.g., Figure 1).

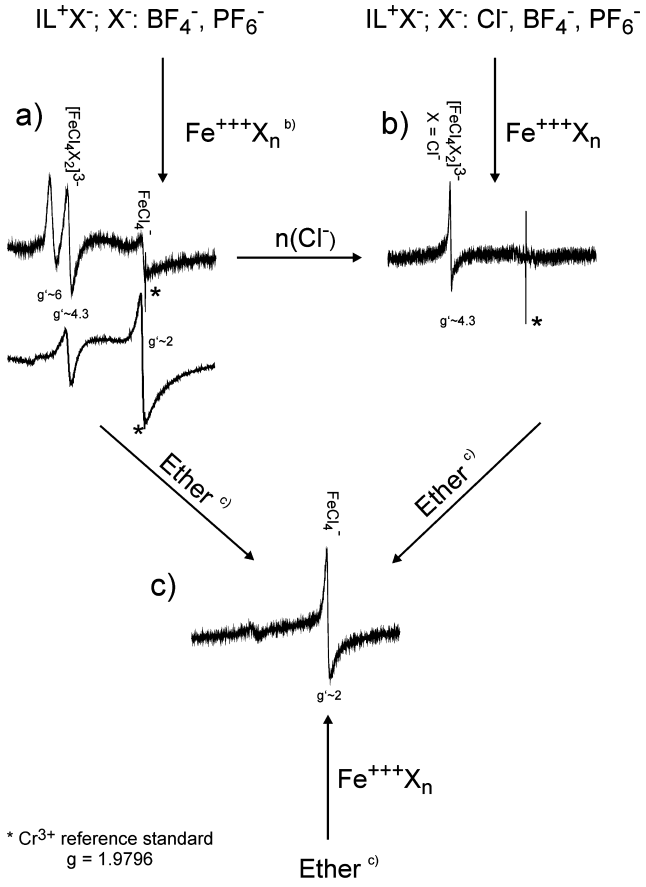

Figure 1. Schematic survey about the interconversion of the Fe^{3+} spin probes in ionic liquids.

- Proof of the molecular control about the properties of the examined ILs and the (partly reactive) dissolved transition metal ions.
- Finding the specifics of the interactions in ILs compared to solutions of Fe(III) species in conventional solvents.
- Proof for the chemical reactions of $FeCl_3$ or $FeCl_4^-$, respectively, with the constituents of the systems as a consequence of the changing the properties of the ILs due to the variation of the substituent at the imidazolium cation and the corresponding anion (BF_4^-, PF_6^-, Cl^-, and $FeCl_4^-$).
- Comparison of the results with those obtained on using conventional nitroxyl radicals as spin probes.
- Proof for the general model character of the application of the "model kit" for the interpretation of other complex Fe^{3+} ions containing systems and frozen solutions of Fe^{3+} species.

Altogether it will be demonstrated that the transition metal ion probes act as "observers which take part" without loosing their character of reporters.

EXPERIMENTAL SECTION

The ESR spectra have been recorded using the X band spectrometer ERS 300 (ZWG Berlin; Magnettech Ltd. Berlin) equipped with a quartz Dewar for measurements at 77 K. The parameters for the device have been set to 2 mW power, 100 kHz modulation, and B_0 in the range from 50 to 5000 G.

The ILs (see Figure 2) have been synthesized as described in refs 16, 17, and 43 and the literature cited therein and bought

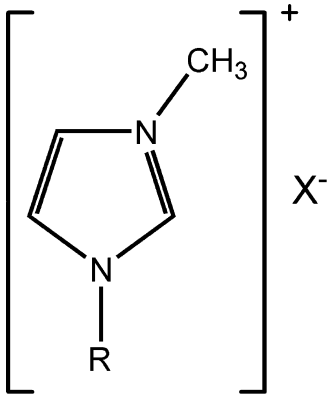

Figure 2. Structure of the imidazolium based ionic liquids (R = methyl−decyl, X^- = Cl^-, BF_4^-, and PF_6^-).

from IoLiTec Ionic Liquids Technologies GmbH, Heilbronn, Germany, as well. All other chemicals were taken from the laboratory, having sufficient purity.

Simulations. In order to get an interpretation of the experimental findings two methods have been used.

(i) Complete simulation of the ESR spectra for the quantitative determination of the coexisting spectral contributions of paramagnetic species exhibiting weak interactions or exchange couplings within the experimental spectra.

(ii) Assignment of these contributions on using model systems such as Butyl-Methyl-Imidazolium Tetrachloroferrate (ButylMImFeCl$_4$), KFeCl$_4$, or NaFeCl$_4$ and other spectroscopic results.

Within the hierarchy of spectra interpretation, diamagnetically diluted paramagnetic single crystals rank first, followed by powder spectra, amorphous systems, isotropic, structured, and frozen solutions.[44,45]

Similarly a hierarchy of spectra interpretation can be established, ranging from the complete simulation based on the Spin-Hamiltonian operators considering perturbation terms up to the fourth and sixth order, respectively, including dynamic effects, up to different phenomenological approaches such as preliminary conclusions obtained from effective g-factors ($g' = h\nu/\beta B$) and uncorrected splittings.

The shape of X-band ESR spectra of Fe(III) in solid matrices is usually characterized by a few intense peaks, superimposed by statistical distributions of zfs parameters. Particularly in ILs with their manifold possibilities of structuring in fluid and solid phases (differently to conventional solvents), these distributions do not complicate the spectra interpretation but are an important source of information about the internal states of these systems.

The values of the zfs parameters as well as their distributions are determined by the number, the chemical nature, and the geometrical arrangement of coordinating atoms at the Fe(III) ions including their local interactions with the matrix (e.g., ImBF$_4$ and ImPF$_6$) and if applicable in matrix compartments ("domains") of different structure and polarity.

dx.doi.org/10.1021/jp403260r | J. Phys. Chem. A 2013, 117, 3960−3971

Table 1. Results of the Simulations of ESR Spectra of Frozen Solutions (77 K) of $FeCl_3$ in ILs[a]

sample		signal position g' ~ 6	g' ~ 4.3	g' ~ 2.4	g' ~ 2
$FeCl_3$-ButylMImBF$_4$	spectrum	-	*va12a23* g: 2.15 ΔB: 200 G b22=3800, db22=5000 intensity: 11 %	*va13a16* g: 2.6,2.3,2.1 ΔB: 1500 G intensity: 67.4 %	*va11a35* g: 2.06,2.06,2.05 ΔB: 250 G b43=2800, db43=1000 intensity: 21.6 %
	band pass filtered	*va14a03* g: 2.15 ΔB: 190 G b20=6000 intensity: 1.4 %	*va12b64* g: 2.13 ΔB: 130 G b22=3800, db22=5000 intensity: 35.8 %	-	*va11a37* g: 2.06,2.06,2.05 ΔB: 140 G b43=2800, db43=1000 intensity: 62.8 %
$FeCl_3$-DecylMImBF$_4$	spectrum	*va14a03* g: 2.15 ΔB: 190 G b20=6000 intensity:	*va12a26* g: 2.1 ΔB: 180 G b22=3800, db22=5000 intensity:	?	*va11a35* g: 2.06,2.06,2.05 ΔB: 250 G b43=2800, db43=1000 intensity:
	band pass filtered	*va14a03* g: 2.15 ΔB: 190 G b20=6000 intensity: 40.8 %	*va12b64* g: 2.13 ΔB: 130 G b22=3800, db22=5000 intensity: 49.2 %	-	*va11a37* g: 2.06,2.06,2.05 ΔB: 140 G b43=2800, db43=1000 intensity: 10.7 %
$FeCl_3$-ButylMImPF$_6$	spectrum	-	*va12a26* g: 2.1 ΔB: 180 G b22=3800, db22=5000 intensity: 8.5 %	*va13a58* g: 2.434,2.434,1.9 ΔB: 1500 G intensity: 55.7 %	*va11a35* g: 2.06,2.06,2.05 ΔB: 250 G b43=2800, db43=1000 intensity: 35.8 %
	band pass filtered	-	*va12b64* g: 2.13 ΔB: 130 G b22=3800, db22=5000 intensity: 34.2 %	-	*va11a37* g: 2.06,2.06,2.05 ΔB: 140 G b43=2800, db43=1000 intensity: 65.8 %
$FeCl_3$-OctylMImPF$_6$	spectrum	-	*va12a26* g: 2.1 ΔB: 180 G b22=3800, db22=5000 intensity: 10.7 %	*va13a58* g: 2.434,2.434,1.9 ΔB: 1500 G intensity: 63.8 %	*va11a35* g: 2.06,2.06,2.05 ΔB: 250 G b43=2800, db43=1000 intensity: 25.5 %
	band pass filtered	-	*va12b64* g: 2.13 ΔB: 130 G b22=3800, db22=5000 intensity: 57.4 %	-	*va11a37* g: 2.06,2.06,2.05 ΔB: 140 G b43=2800, db43=1000 intensity: 42.5 %

[a]The names of the calculated individual subspectra are given in italics; b22, b43, db22, and db43 stand for b_2^2, b_3^4, Δb_2^2, and Δb_3^4, respectively.

The experimental spectra have been calculated by means of the program, described in ref 42, using the spin-Hamilton parameter as given in eq 1

$$\hat{\mathbf{H}} = \beta \cdot \vec{\mathbf{B}}_0 \cdot \vec{\mathbf{S}} + \sum_{m,n} \mathbf{B}_n^m \cdot \mathbf{O}_n^m \tag{1}$$

and the corresponding crystal field potential (eq 2).

$$\mathbf{V} = \sum_{m,n} \mathbf{B}_n^m \cdot \mathbf{O}_n^m = \frac{1}{\mathbf{f}_n} \cdot b_n^m \cdot \mathbf{O}_n^m \tag{2}$$

Examples for the used parameters b_n^m are given in Table 1. The model calculations have been done in order to obtain (i) an assignment of the zfs transitions and similarly (ii) a certain connection to the frequently used semiquantitative interpretation of ESR spectra of Fe^{3+} via g' values. There are many cases of ESR spectra with unknown values for b_0^2 (or D, respectively),[46] thus in Figures 3 and 4 the results of spectra calculations for different b_0^2 values are summarized showing the influence of varying values of parameter b_2^2 (or E, respectively).[47] If the ratio E/D is around 1/3 (or $b_2^2/b_0^2 \approx 1$), the main intensity in X band will be found at about 1500 G ($g' \approx 4.3$), accompanied by a less intense component between 700 and 900 G (or g' between 7.2 and 9.2). On increasing the ratio b_2^2/b_0^2 the main intensity shifts toward higher field values. Above a certain threshold value the spectral pattern nearly does not change further due to the fact that the field of the Fe(III) ions dominates now the axis of quantization and the splitting of the spin levels. Derived from the threshold values it will be possible to conclude to the approximate value of the largest zfs parameter.

RESULTS

Figure 5 displays a typical ESR spectrum of $FeCl_3$ dissolved in an IL (here ButylMImBF$_4$) recorded at 297 K. It shows a broad line at $g' \approx 2$ with a broad low field shoulder. The g' factors correspond with the expectation for Fe(III) ions, but a further differentiation is nearly impossible at room temperature even on using differently substituted ILs, whereas Figure 2b shows

dx.doi.org/10.1021/jp403260r | J. Phys. Chem. A 2013, 117, 3960−3971

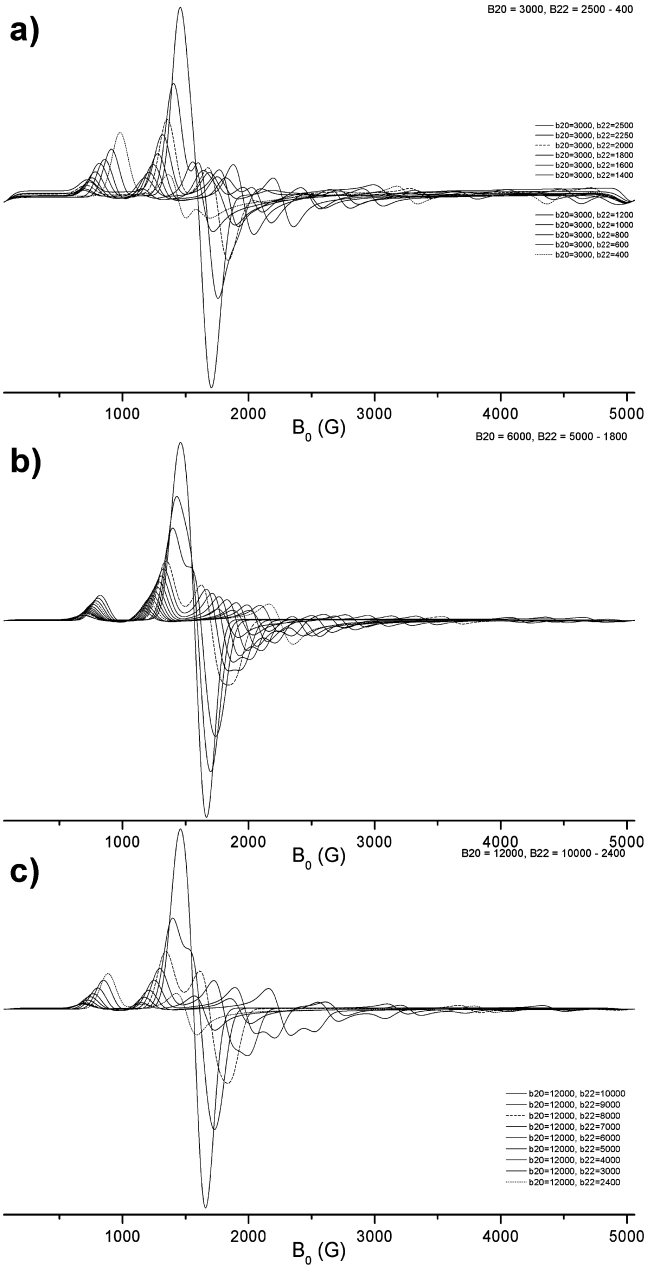

Figure 3. Simulations of the ESR spectra of Fe(III) ions in crystal electric fields of different symmetry as determined by the values of the spin-coupling parameters b_0^2 and b_2^2 (see eqs 1 and 2).

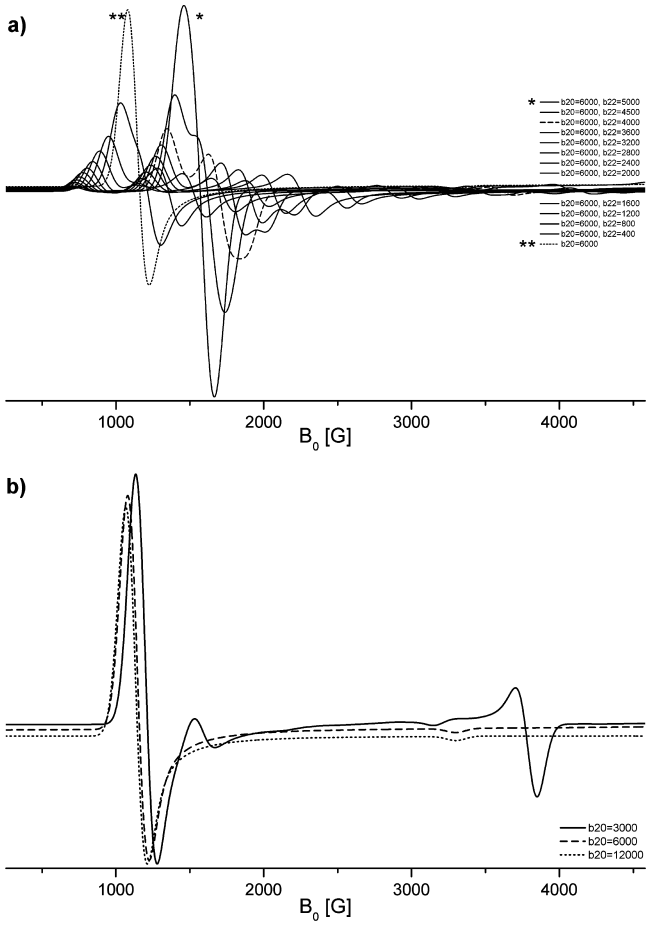

Figure 4. Simulations of the ESR spectra of Fe(III) ions in crystal electric fields of different symmetry with particular consideration of the signal intensity around 1000 G ($g' \approx 6$).

the ESR spectrum at 77 K. In this case a much stronger differentiated spectrum can be observed. The small letters indicate areas, which show characteristic changes in dependence on the structure of the used IL. Generally, this X band ESR spectrum can be considered as typical for Fe(III)Cl_x probes in ILs.

A closer look shows a falling zero line in the low field. This trend has been found in many systems of ILs with $FeCl_3$/$FeCl_4^-$ additions. Comparing that with X band spectra of low valent Fe species[46] as well as Fe^0 nanopowders suspended in ILs, that part of the spectrum could be assigned to the redox product between $FeCl_3$ and ILs.

Particularly on using ILs with BF_4^- anion, the intensity of the spectrum in region c is influenced by the length of the side chain as can be seen in Figure 6. Because the ESR spectra are usually displayed in the first derivative, the intensity in region e does not seem to be important. However, in most cases it is the main part of the integral intensity (see Table 1), which is caused by aggregation of $FeCl_x$ (e.g., $FeCl_4^-$) species.[47]

By means of Fourier filtering the broad line was at least discriminated in order to verify the signal assignment (see Figure 6b).

For signal assignment and for understanding the effects of changing composition of the ILs, including varying the anions, we followed the procedure according to Figure 1. For probing $FeCl_3$, $FeCl_4^-$ with the cations Na^+, K^+, and ButylMIm$^+$ have been used. Moreover, we made use of the well-known possibility to extract $HFeCl_4$ and $FeCl_3$ (Fe_2Cl_6) by means of organic solvents, in particular with ether or hexamethylphosphorous triamide (HMPT). As in Figure 1 shown, the different species can be changed reversibly.

An interesting case of the changing shape of the ESR spectra for $FeCl_3$/$ILBF_4$ at 77 K is shown in Figure 6a. It is remarkable that with increasing length of the side chain at the imidazolium ring the signal intensity of signal at $g' \approx 6$ ($\mathbf{B}_0 \approx 1000$ G) increases, whereas that at $g' \approx 2$ ($\mathbf{B}_0 \approx 3300$ G) decreases. After Fourier filtering (Figure 6b) the effect can be observed even more clearly and the transitions could be quantified based on the respective spectrum simulations (see Table 1).

Figure 7 shows the respective spectra for the system $FeCl_3$/$ImPF_6$. The missing signals at $g' \approx 6$ (region c) and the larger

dx.doi.org/10.1021/jp403260r | J. Phys. Chem. A 2013, 117, 3960−3971

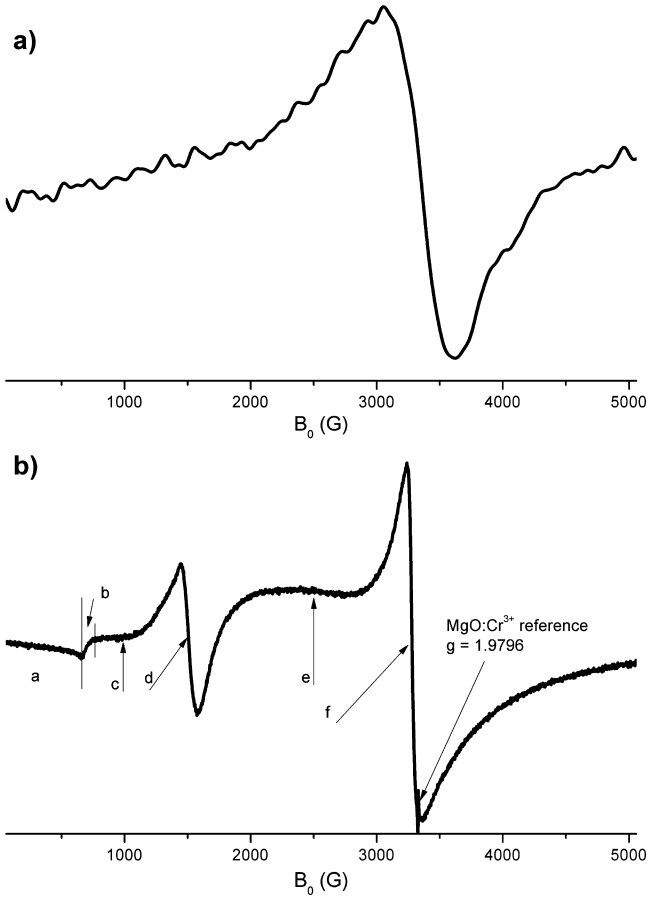

Figure 5. Experimental spectra of $FeCl_3$ in $ButylMImBF_4$ at room temperature (a) and 77 K (b). As an example in the spectrum at 77 K those regions are marked where the typical Fe^{3+} species deliver a spectral contribution.

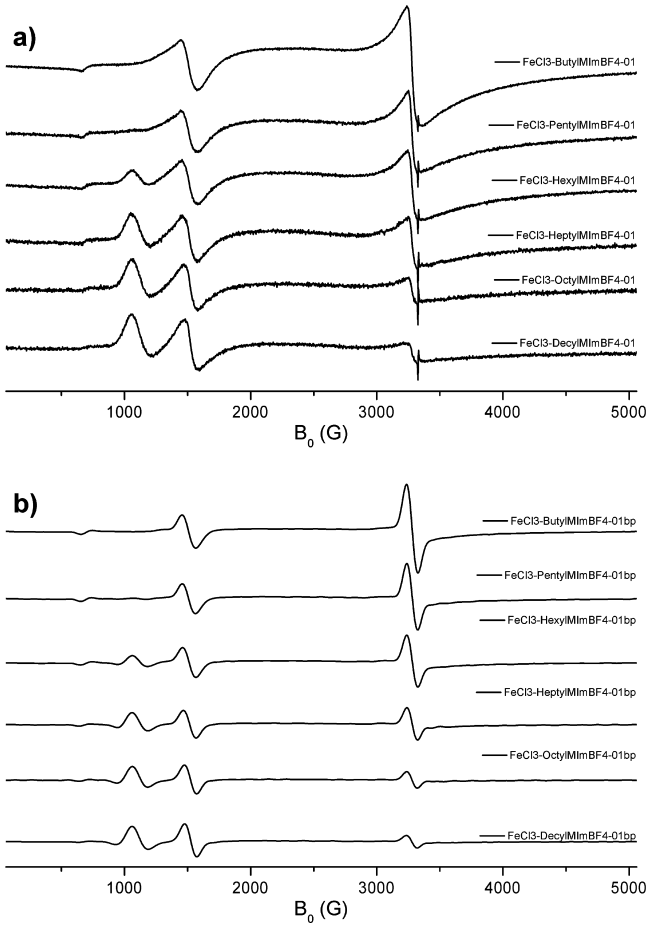

Figure 6. Experimental spectra of $FeCl_3$ in R_1-$MImBF_4$ (a) and (b) Fourier filtered.

line widths of the signals at $g' \approx 2$ (region f) are peculiar for that system.

On using $FeCl_4^-$ instead of $FeCl_3$ gave similar spectra as displayed in Figures 6 and 7, though in region c no signals could be observed. As shown in Figure 1, the addition of Cl^- ions (e.g., in form of a saturated aqueous solution of LiCl) leads to the characteristic spectral shape with a dominating intensity at $g' \approx 4.3$. Such spectra are well described (e.g., Fe^{3+} ions in glasses or similar system without translation symmetry).[41,48] Up to now there are only a few attempts of complete simulations of such spectra in order to make signal assignments.[41]

The spectra of frozen solutions of $FeCl_3$ or $FeCl_4^-$ in ether and other nonpolar organic solvents (e.g., HMPT) are characterized by comparably small line widths in the region f around $g' \approx 2$ and small intensities in the low field (regions b–d). Comparing our finding with ESR examinations of doped single crystals,[49] these signals can be assigned to $FeCl_4^-$ ions as it could be found with phenomenological extraction experiments[34,35] in combination with UV–visible spectroscopy.

Figures 8–11 display the results of the complete simulations for the experimental spectra of selected $FeCl_3$/IL systems in their original form and after Fourier filtering. The simulations have been carried out using a certain "model kit" principle in order (i) to reproduce the overall spectra by means of individual shares of subspectra and (ii) to create a basis for the application to more general Fe(III) problems as they appear in solid state chemistry and physics.

Figure 8a displays the decomposition of the experimental spectra of the systems $FeCl_3$/$ButylMImBF_4$ and $FeCl_3$/$DecylMImBF_4$ in subspectra, which had been obtained from simulation. For that, parts of the signal at $g' \approx 2$ have been simulated according to values for the zfs parameters of the $FeCl_4^-$ ion from the literature.[49] The identity of that species has been proved by additional experiments (see experimental descriptions below). The statistical distribution of the cubic splitting parameters (see Tables 1 and 2) has been fitted to the experimental spectrum. The spectral difference between these two IL systems seems to be relatively large and should be attributed to the changes in the side chain on the imidazolium ring, but on using the "model kit" the spectra could be fitted effortless.

After Fourier filtering (Figure 9b) the differences between the two systems can be seen even more clearly, in particular the increase in intensity of the low field signal and the loss at around $g' \approx 2$.

For Figures 10 and 11 these considerations are repeated for similar systems where the cation of the ILs is PF_6^- instead of BF_4^- and the side chains at the imidazolium ring range from butyl to octyl. Even in these cases Fourier filtering gives the opportunity to see the changes in the spectra more clearly and allows the quantification of the spectral contributions of the involved Fe(III) species.

The integral contributions in the range of the effective g' factors 6, 4.3, and 2 (ranges c, d, and f in Figure 5) as function of the length of the side chain (number of C atoms) are

dx.doi.org/10.1021/jp403260r | J. Phys. Chem. A 2013, 117, 3960–3971

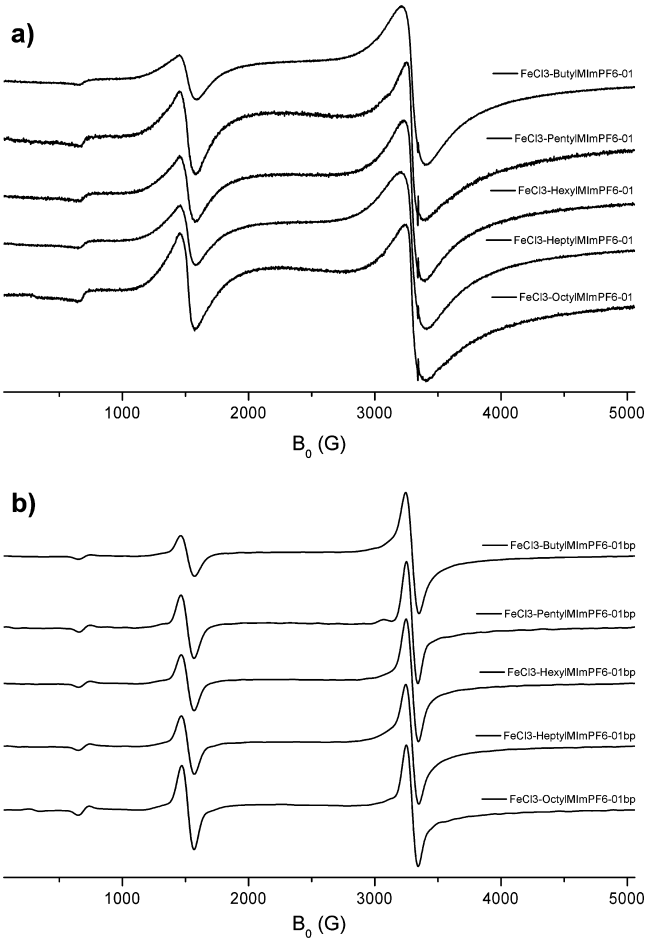

Figure 7. Experimental spectra of $FeCl_3$ in R_1-$MImPF_6$ (a) and (b) Fourier filtered.

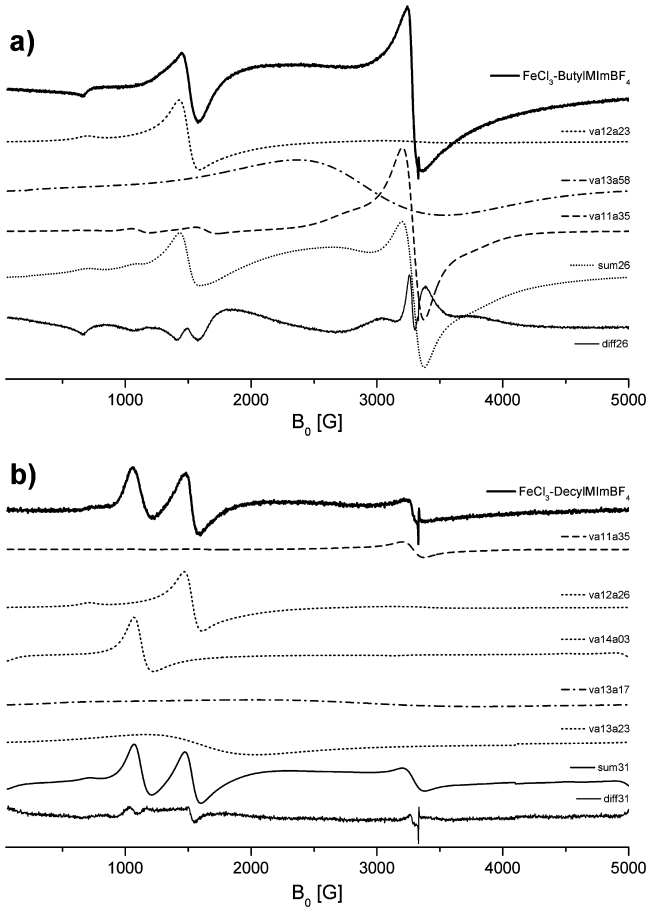

Figure 8. Comparison of the calculated subspectra for $FeCl_3$ in R_1-$MImBF_4$ (R_1 = butyl (a) and decyl (b); the simulation parameters for the subspectra can be found in Table 1).

displayed in Figure 12. In case of the BF_4^- anion we can observe the increase of the contribution to the overall signal intensity at $g' \approx 6$ (see also Figure 4b) and the decrease at $g' \approx 2$, and in the case of PF_6^- we observe similar trends except the missing signal at $g' \approx 6$.

Figure 13 shows the experimental ESR spectrum of the system $FeCl_3$/ether and the results of the simulation as well. As expected the signal in region f ($g' \approx 2$) has a much smaller line width, i.e., is mainly caused by spectral contributions of the anion $FeCl_4^-$.

Another interesting spectrum is displayed in Figure 14. The addition of Cl^- (and H_2O) leads to a total shift of the ESR signal intensity to region d, i.e., $g' \approx 4.3$.

The results of all simulations are summarized in Tables 1 and 2.

Additional Means for Assignment. The addition of ether or hexamethylphosphoric triamide (HMPT) to solutions of $FeCl_3$/R-$MImBF_4$ or $FeCl_3$/R-$MImPF_6$ leads to greater lucidity of the solutions. This is caused by a reduction of the formation of associates (reduction of signal intensity at $g' \approx 2.4$). After filtration and freezing the ethereal solution (or HMPT) the typical signals at $g' \approx 4.3$ and 2 will be transferred to the typical $FeCl_4^-$ signal at $g' \approx 2$ (this is more or less reversible). On using solvents like methanol, ethanol, DMSO, etc. a signal around $g' \approx 4.3$ appears, which indicates the participation of solvent molecules in the coordination of Fe(III). In contrast to that, the extraction with ether (see Figure 13) or HMPT proves the presence of $FeCl_4^-$ in an extractable form in the IL solution. This statement is supported by examination on solutions of $FeCl_3$ and $KFeCl_4$ in ether or HMPT, which delivered the ESR response of $FeCl_4^-$ (see zfs parameters in Table 1).

Another means of assignment of signals in spectra of $FeCl_3$/ILs has been the examination of ILs with the anion $FeCl_4^-$ (e.g., as diluted system $ButylMImFeCl_4$), solutions of $KFeCl_4$ or $NaFeCl_4$ in ILs, ether, or HMPT. It could be shown, that on using ILs as solvent spectra could be observed similar to those of $FeCl_3$/ILs systems as shown in Figure 13. However, only traces of a signal in region c ($g \approx 6$) could be observed. Interestingly, this signal appeared immediately on adding $ImBF_4$ to solutions of $FeCl_3$/$ImPF_6$.

Changing to other anions has been done e.g. by adding a saturated aqueous LiCl solution. Under these conditions Fe(III) species have been formed which are similar to those of the system $FeCl_3$/ButylMImCl, and whose ESR responses are signals with relatively small line widths in regions b and d ($g' \approx 9.5$ and 4.3; Figure 14). Even from these systems $FeCl_4^-$ could be extracted by means of ether or HMPT.

Comparison with Results Obtained from the System $Fe(ClO_4)_3 \cdot 9H_2O$/ILs. All up mentioned examples are related to $FeCl_3$ or $FeCl_4^-$ probes in ILs. By means of complexing agents with "other" structures (e.g., acac, edta) and $Fe(ClO_4)_3 \cdot 9H_2O$ it has been checked if the observed effects are related to binding interactions with Cl^- ligands of the spin probes. In the case of acac, edta, etc. discrete signals in region b–d (see Figure 5)

dx.doi.org/10.1021/jp403260r | J. Phys. Chem. A 2013, 117, 3960–3971

Table 2. Calculated Integral ESR Intensities [%] of the Contributing Components at $g' \approx 6$, 4.3, 2.6, and 2 to the Overall Spectra in the Systems $FeCl_3/R_1$-$MImBF_4$ and $FeCl_3/R_1$-$MImPF_6$

R_1	$g \approx 6$	$g \approx 4.3$	$g \approx 2.6$	$g \approx 2$
		R_1-$MImBF_4$		
butyl	0	11.03	67.39	21.58
pentyl	0.24	9.52	66.37	23.87
hexyl	2.93	13.34	59.22	24.51
heptyl	3.08	8.47	72.84	15.61
octyl	4.76	18.27	68.74	8.22
decyl	5.78	19.25	69.21	5.76
		R_1-$MImBF_4$ (band-pass filtered)		
butyl	1.45	35.77		62.81
pentyl	0.77	45.72		53.52
hexyl	16.17	34.88		36.13
heptyl	30	41.05		33.11
octyl	52.34	67		22.34
decyl	40.82	49.2		10.66
		R_1-$MImPF_6$		
butyl		8.47	55.68	35.85
pentyl		15.03	59.98	24.99
hexyl		12.33	55.21	32.47
heptyl		11.85	48.98	39.17
octyl		10.71	63.78	25.51
		R_1-$MImPF_6$ (band-pass filtered)		
butyl		34.18		65.82
pentyl		56.12		43.88
hexyl		30.81		35.36
heptyl		35.63		34.05
octyl		57.42		42.58

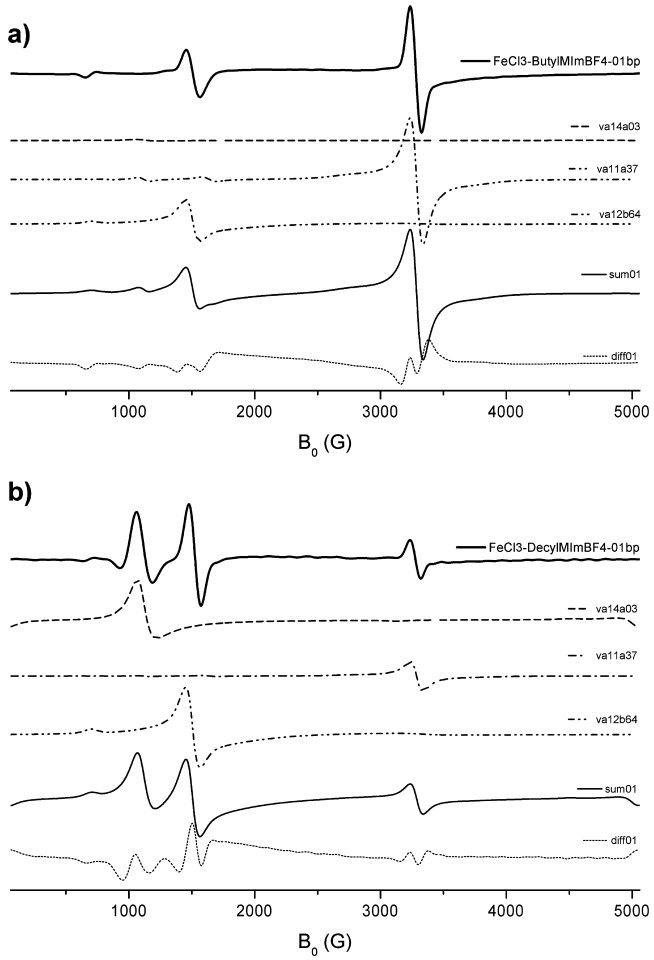

Figure 9. Comparison of the calculated subspectra for $FeCl_3$ in R_1-$MImBF_4$ (R_1 = butyl (a) and decyl (b)) after Fourier filtering (the simulation parameters for the subspectra can be found in Table 1).

have been found. With Fe(III) perchlorate signals around $g' \approx 2$ of a certain line width (700−1000 G) could be seen starting with a hexyl side chain at the imidazolium cation. For $ButylMImBF_4$ and $PentylMImBF_4$ the signals could not be evaluated due to their very broad lines. With increasing length of the side chain (heptyl to decyl) discrete signals in region b to d ($g' \approx 9.5$ and 4.3) could be observed.

Preliminary Summary of the Experimental Findings and Simulations. On dissolving the Fe(III) probes $FeCl_3$, $ImFeCl_4$, $KFeCl_4$, and $NaFeCl_4$ in the selected ILs comparatively symmetrical species of the type $FeCl_4^-$ (ESR detection of $S = 5/2$; zfs parameters see Table 1), aggregates with broad lines around $g' \approx 2.4$, and axially or rhombically, respectively, distorted species in the low field ($g' \approx 9.5$−4.3) are formed.

The shape of the X band ESR spectra of the examined $FeCl_3$/IL and $FeCl_4^-$/IL systems can be considered to be typical for such systems.

They can be (reversibly) changed to $FeCl_4^-$ by means of ether and HMPT.

Generally these spectral patterns do not coincide with those from simple liquids.

The up to now findings point to the statement, that the properties of the resulting IL solutions can be adapted to the establishments of equilibria of dissolved species by purposeful molecular changes (variation of the substitution at the imidazolium cation, kind of anions, etc.) together with the formation of fluctuating domains of different polarity in the solvent system.

It is noticeable that the variation of the length of the side chain at the imidazolium cation controls the ratio of the spectral contributions at $g' \approx 6$, 4.3, and 2. If the chain length is short (e.g., in $ButylMImBF_4$ or $ButylMImPF_6$) the species $FeCl_4^-$ dominates the spectrum of the $g' \approx 2$ region. With increasing chain length the share of polar compartments decreases in the IL.

Table 3. Simulation Parameters for the Subspectra As Used for the Systems $FeCl_3$/Ether and $FeCl_3$/sat. LiCl

subspectrum	g	ΔB [G]	fine structure parameters
va11a45	2.06, 2.06, 2.05	125	$b_3^4 = 2800$, $\Delta b_3^4 = 300$
va11a51	2.06, 2.06, 2.05	250	$b_2^2 = 3000$, $b_3^4 = 6000$, $\Delta b_3^4 = 3000$
va12a53	2.064	53	$b_2^2 = 6000$,$\Delta b_2^2 = 4900$
va13a56	2.434	1000	−
va19a88	2.06	110	$b_0^2 = 3000$, $b_2^2 = 2500$, $\Delta b_2^2 = 500$

dx.doi.org/10.1021/jp403260r | J. Phys. Chem. A 2013, 117, 3960−3971

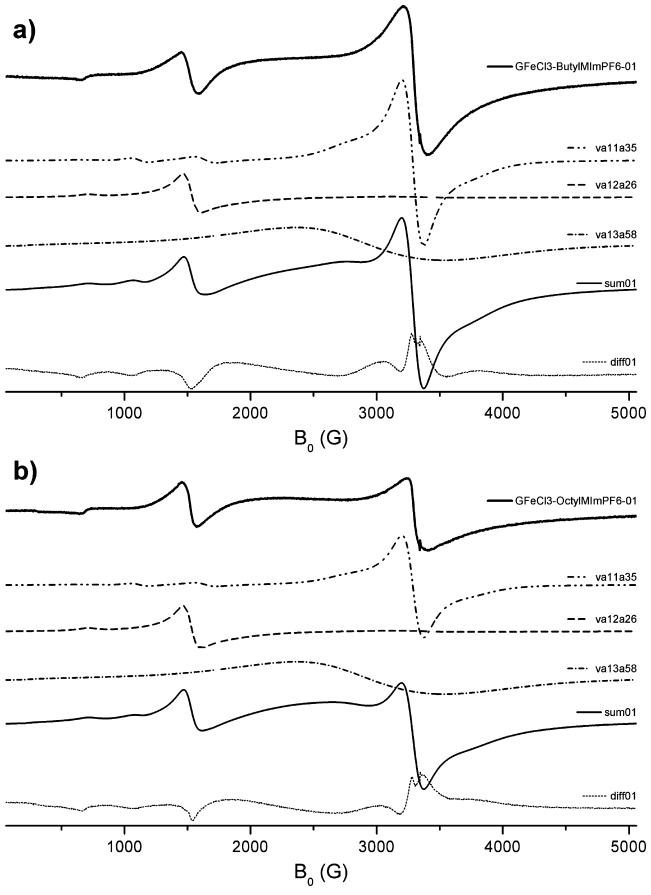

Figure 10. Comparison of the calculated subspectra for $FeCl_3$ in R_1-$MImPF_6$ (R_1 = butyl (a) and octyl (b); the simulation parameters for the subspectra can be found in Table 1).

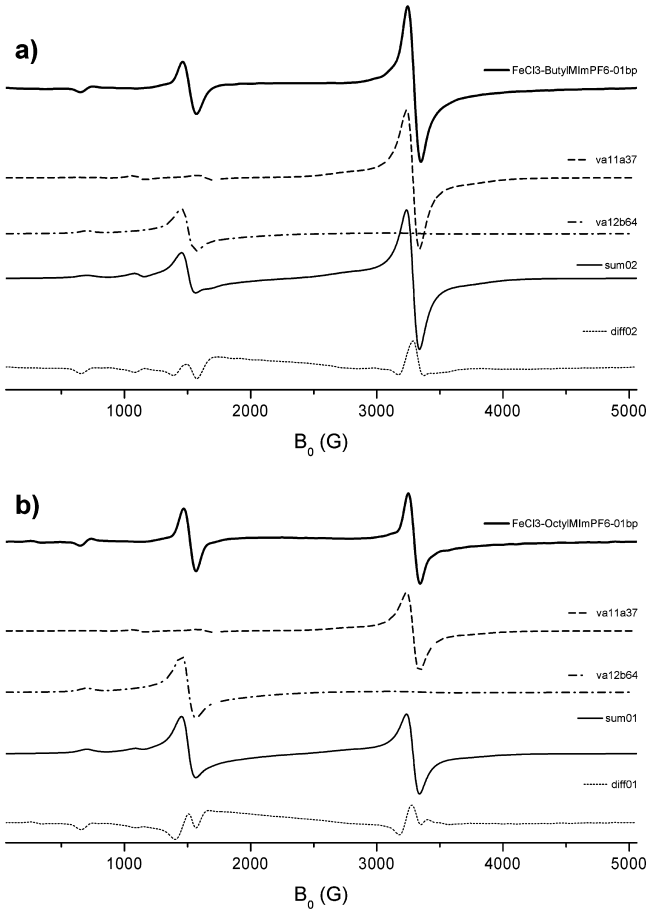

Figure 11. Comparison of the calculated subspectra for $FeCl_3$ in R_1-$MImPF_6$ (R_1 = butyl (a) and octyl (b)) after Fourier filtering (the simulation parameters for the subspectra can be found in Table 1).

Only on using BF_4^- anions $FeCl_3$ caused an increase of the signal intensity at $g' \approx 6$ (strongly axially distorted polyhedra; see Figure 4). The addition of BF_4^- to $FeCl_3/ImPF_6$ solutions brings forth the side chain length-dependent signal at $g' \approx 6$, too.

By means of extraction the existence of $FeCl_4^-$ ions can be proved for all examined $FeCl_3$/IL systems.

DISCUSSION

Contrary to the increasing number of examinations regarding the properties and applications of ionic liquids (ILs) in physics, chemistry, and biology, ESR investigations of paramagnetic compounds in ILs are relatively rare.[16,17,19,50] They have been carried out mainly using nitroxyl radicals for determining microviscosity, micropolarity, microheterogeneity, etc. of solutions, pharmaceutical, and biological objects, for studying the course of radicalic polymerization reactions.[43] Those nitroxyl radicals are of known polarity and structure. Moreover, they do not change much in their surrounding, e.g., due do the acting of weak Coulomb interactions or the establishment of hydrogen bridges. At temperatures above 300 K small changes in the spin density distribution and thus in the value of the hyperfine couplings occur by thermal fluctuations in the sphere of surrounding molecules of the solvent. That means these spin probes take over the task of "observers" and deliver information about the surrounding medium.[11] The combination of examinations on using spin probes of different structures (including their isotopic patterns) allows conclusions concerning the microheterogeneities in the structure of solutions.[10−15]

Due to their physical and chemical properties the usage of Fe^{3+} ($S = 5/2$) ions as spin probes is particularly challenging. Their ESR fine structure serves as an unique source of information and their chemical changes make them to "observers" which take part. Thus, it was possible to observe discrete ESR signals in the range of effective g' factors of 18, 9.5, 6, 4.3, 2.4, and 2 depending on the structure of the ILs and additional components. Moreover, it was possible to simulate these spectra and to quantify their contribution to the respective overall spectrum. The ESR examinations have been carried out at 77 K in order to reduce the influence of the thermal fluctuations of the microstructures (and therefore the zfs and the $\Delta\mathbf{B}$ values) significantly.

Only a small fraction of natural iron is characterized by having a nuclear spin different from zero (^{57}Fe: $I = 1/2$, natural abundance 2.19%). This and the line widths (i.e., the splittings of the ^{57}Fe are covered by the broad lines of ^{56}Fe with $I = 0$) lead to the possibility to do the simulation by means of the Spin-Hamiltonian $\hat{\mathbf{H}}$ with $S = 5/2$ and $I = 0$ according to eq 1.

As an example, the influence of the fine structure parameters b_0^2 and b_2^{2S0} is demonstrated in Figure 3 and similarly it shows the applicability of the procedure for the simulation of the experimental spectra (Figures 8−11).

The habit of the spectra reveals the formation and stabilization of different Fe(III) species from $FeCl_3$ as well as

dx.doi.org/10.1021/jp403260r | J. Phys. Chem. A 2013, 117, 3960−3971

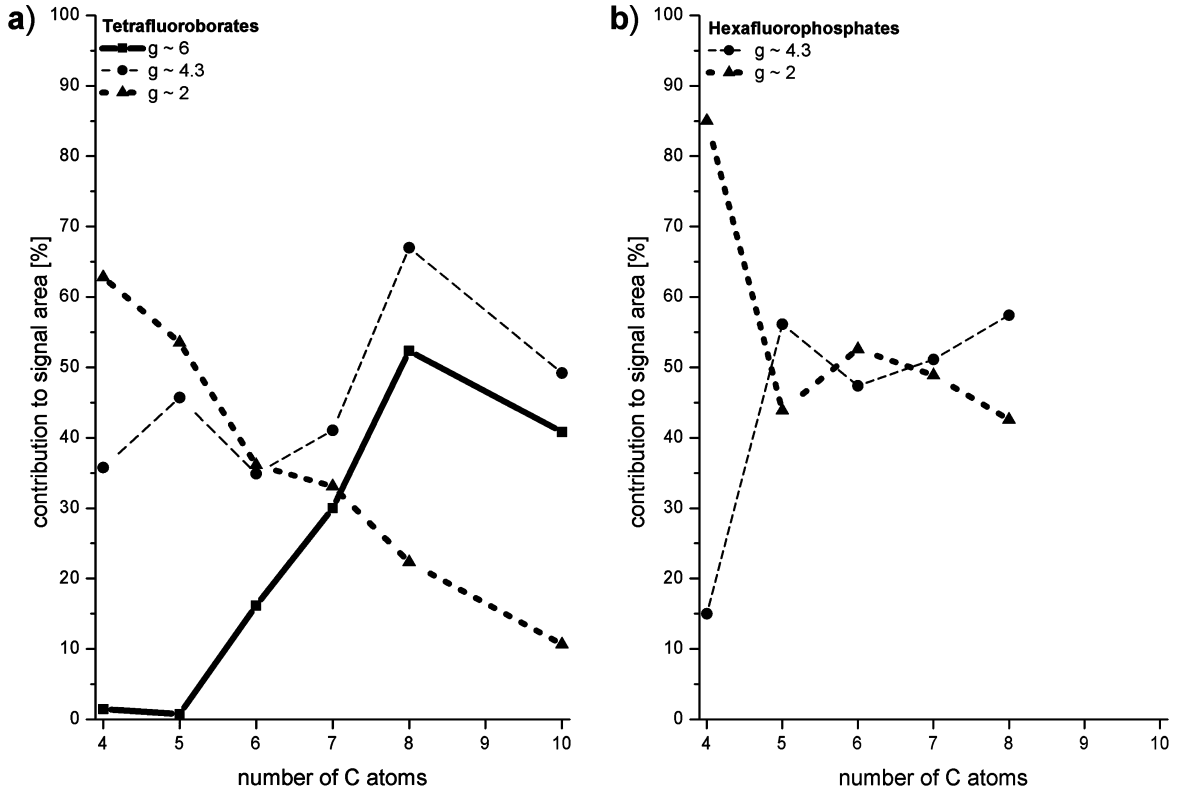

Figure 12. Contributions of the subspectra to the overall spectra as a function of the length of the side chain for $FeCl_3$ in ILs with the anions BF_4^- (a) and PF_6^- (b).

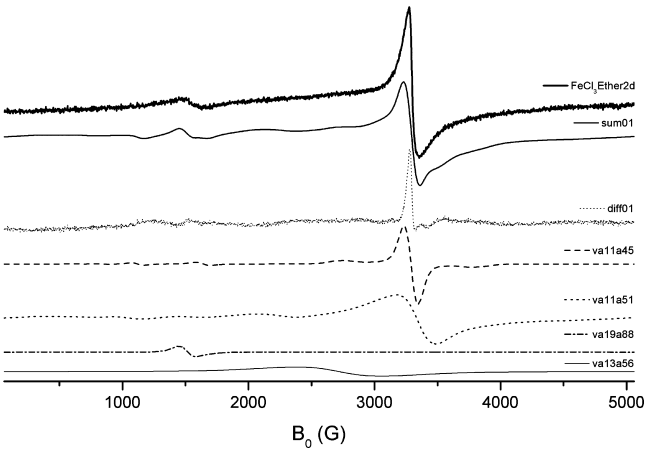

Figure 13. Contributions of the subspectra to the spectrum of $FeCl_3$ in ether at 77 K (for simulation details see Table 3).

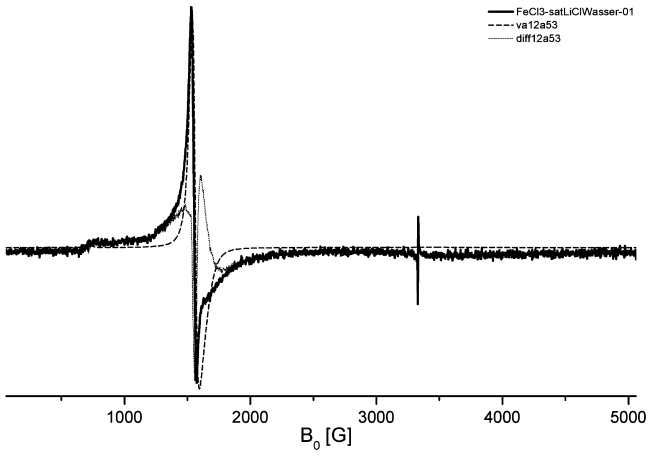

Figure 14. Contributions of the subspectra to the spectrum of $FeCl_3$ in a saturated aqueous LiCl solution at 77 K (for simulation details see Table 3).

$FeCl_4^-$ existing in ILs. Kind and concentration of these species depend on the substitution of the IL cation and the type of anion (BF_4^-, PF_6^-, and Cl^-). Generally, the region $g' \approx 2$ (see Table 1) is determined by $FeCl_4^-$ and its states of aggregation[47] with line widths ≥250 G. The contributions of further states of aggregations can be observed around $g' \approx 2.4$ which originate from species with $g' \approx 4.3$ due to spin exchange (or their predecessors). The general trend toward an increase of the percent contribution of the signal intensity at $g' \approx 4.3$ in relation to that at $g' \approx 2$ (see Figure 13) is caused by chemical and physical effects in the substituted ILs: with increasing length of the side chain at the imidazolium cation the tendency to form nonpolar domains increases, too.

The assignment of the Fe^{3+} signals, obtained from the measurements of frozen solutions in ILs and characterized by their parameters g_i, ΔB_i, b_0^2, and b_2^2 as well as the corresponding statistical distributions of the zfs parameters, has been done using chemical considerations (see Figure 1) and further chemical and spectroscopic experiments.

Due to their competing inner interactions ILs possess a complex structure.[51,52] They allow a molecular control over the properties of the liquid state. This will be mainly achieved by functionalizing the used cation. At least one of the ions should be amphiphilic with respect to charged and uncharged components of the liquid system. As a consequence the segregation of ionic and nonionic components, self-organ-

dx.doi.org/10.1021/jp403260r | J. Phys. Chem. A 2013, 117, 3960−3971

ization, the formation of nanostructures and mesophases by combined action of ionic interactions and hydrogen bridges are possible. Under chemical considerations the unique properties allow the progress of unusual chemical reactions, which are impossible in neutral solvent of comparable polarity.[53] Up to now not much is known about the influence of the structural properties of the ILs on course of chemical reactions. Among others that means the allocations of reaction spaces in form of polar and nonpolar domains.[54−56] In the ILs used here this is caused by the hydrophobic nature of alkyl side chain of the imidazolium cation.

The eqs 3−8 show a possible sequence of adaptions of Fe(III) species to existing structural domains in the ILs. Equation 8 expresses the exchange of BF_4^- anions in ILs by $FeCl_4^-$.

$$2FeCl_3 \rightleftharpoons Fe_2Cl_6 \quad (3)$$

$$Fe_2Cl_6 \rightleftharpoons FeCl_4^- + FeCl_2^+ \quad (4)$$

$$FeCl_4^- + H^+ \rightleftharpoons HFeCl_4 \quad (5)$$

$$FeCl_4^- + FeCl_3 \rightleftharpoons Fe_2Cl_7^- \quad (6)$$

$$2FeCl_4^- \rightleftharpoons \text{dimers} \quad (7)$$

$$FeCl_4^- + BF_4^- \rightleftharpoons BF_4^- + FeCl_4^- \quad (8)$$

On extending the side chain the average distance between the charged particles increases, the formation of species with $g' \approx 4.3$ is preferred, and spin exchange coupled aggregates $\{Fe^{3+}-X-Fe^{3+}\}$ can partly dissociate and the spectral intensity at $g' \geq 2.0$ decreases. The local polarity decreases, nonpolar domains gain weight.

At 77 K and increasing length of the side chain glass-like states are formed. The entanglement of the side chains contributes to the glass-like state. With that the probability of the formation of rhombically distorted polyeder spaces for Fe^{3+} generally increases.[41,48]

With increasing length of the side chain the number of nonpolar domains increases.[57] This is e.g. indicated by the fact that dehydration reactions are inhibited by pseudo encapsulation effects. In the reverse case reactions with H_2O (here according to eqs 9 to 13) are favored because of decreasing polar domains; that is, the concentration of polar domains is rising and the hydration reactions take place with higher probability.

$$FeCl_4^- + 2H_2O \rightleftharpoons \{FeCl_4(H_2O)_2\}^- \quad (9)$$

$$FeCl_2^+ + H_2O \rightleftharpoons H^+ + \{FeCl_2OH\} \quad (10)$$

$$2\{FeCl_2OH\} \rightleftharpoons \{FeCl_2OFeCl_2\} + H_2O \quad (11)$$

$$\{FeCl_2OH\} + 3H_2O \rightleftharpoons Fe(H_2O)_3Cl_2OH \quad (12)$$

$$FeCl_2^+ + 4H_2O \rightleftharpoons FeCl_2(OH)_4^+ \quad (13)$$

Consequently, the increasing length of the side chain leads to a decreasing ESR intensity at $g' \approx 2$ while the signal intensity in the low field increases (see Figure 6). This effect is strongest with the anion BF_4^-. Under these conditions $FeCl_4^-$ can substitute BF_4^- in the IL manifold. The above-mentioned reactions with H_2O require only a small concentration of water. Excess or complete absence of water change the picture completely.

The above-mentioned effects, in particular that via the length of the side chain, are not limited to the systems $ImBF_4$ and $ImPF_6$. In solutions of $Fe(ClO_4)_3 \cdot 9H_2O$ the increase of the signal at $g' \approx 4.3$ can be observed with increasing chain length, i.e. the Fe^{3+} ions are stabilized in rhombically distorted coordination octahedrons in polar domains under involvement of the anions of the ILs as well as traces of water. As shown in Figure 6 the probability to find a signal around $g' \approx 6$ (i.e., the formation of Fe^{3+} octahedrons with strongly axial distortion[58,59]) increases by a combined effect of chain length and BF_4^- anions. The influence of the BF_4^- anion could be shown by adding $ImBF_4$ to the system $ImPF_6/FeCl_3$. Again a reaction with H_2O in the polar domains, which get smaller, is needed (e.g., in the formation of $\{Im[FeCl_4(H_2O)_2]\}$. However, the effect mainly depends on the educt $FeCl_3$. The small signal at $g' \approx 6$ disappears on adding small amounts of water.

Discrete ESR signals could be observed at 77 K. They could be assigned to different regional domains in the ILs and the Fe^{3+} species, formed in them, could be quantitatively assessed. The synchronous observation of the different coexisting species was possible. Fe^{3+} ions interacting with Cl^- and small amounts of water have been shown to be "adaptive spin probes" in ILs. The Janus face of the Fe^{3+} species formed in the polar and nonpolar domains of the ILs has been shown to be an important source of information for characterizing the heterogeneities of the IL structures, which could observed only incompletely with classical spin probes of the NO• type.[16,17]

Altogether all of the observed findings are up to now not published in the literature.

The purposeful changes of the structure of the Fe^{3+} probes in different polar reaction regions of the ILs and their synchronous detection could be the basis for future examinations of solvent controlled chemical reactions on taking part of paramagnetic molecules (e.g., free radicals and transition metal complexes).

■ CONCLUSIONS

$FeCl_3$ and $FeCl_4^-$ are sensitive probes for determining the local structure of ILs. They are identifiable, extractable, and transferable probes and can be adapted to local physical and chemical peculiarities of the compartments of the ILS. Thus, a purposefully local exchange of ligands and anions can be induced which leads to the coexistence of different iron species. This not only leads to new insights into the complex structure of ILs but in principal offers new opportunities for the synthesis of complex iron species.

The analysis of the spectra by means of the "model kit" for the interpretation of the experimental findings can be directly applied to the analysis of other complex spectra of Fe(III) in frozen solutions or the solid state, despite not always the local structures can be controlled on a molecular level.

In comparison to spin probes with $S = 1/2$ (e.g., NO• probes) the content of information is clearly higher on using the Fe(III) probes ($S = 5/2$), because the fine structure sensitively responds to changes in the surrounding. That per se known effect has been used for the recent work by applying the reversibly changeable and adaptable probe $FeCl_4^-$.

■ AUTHOR INFORMATION

Corresponding Author

*E-mail: wfh@zedat.fu-berlin.de.

Notes

The authors declare no competing financial interest.

■ ACKNOWLEDGMENTS

The authors would like to thank A. Zehl for her support on recording the manifold of ESR spectra and J. Y. Buzaré, G. Silly, and G. Scholz for providing the basis for the spectra simulations.

■ REFERENCES

(1) McCrary, P. D.; Beasley, P. A.; Cojocaru, O. A.; Schneider, S.; Hawkins, T. W.; Perez, J. P. L.; McMahon, B. W.; Pfeil, M.; Boatz, J. A.; Anderson, S. L.; Son, S. F.; Rogers, R. D. Hypergolic ionic liquids to mill, suspend, and ignite boron nanoparticles. *Chem. Commun.* **2012**, *48*, 4311−4313.

(2) Bica, K.; Gärtner, P.; Gritsch, P. J.; Ressmann, A. K.; Schröder, C.; Zirbs, R. Micellar catalysis in aqueous-ionic liquid systems. *Chem. Commun.* **2012**, *48*, 5013−5015.

(3) Gutel, T.; Santini, C. C.; Philippot, K.; Padua, A.; Pelzer, K.; Chaudret, B.; Chauvin, Y.; Basset, J.-M. Organized 3D-alkyl imidazolium ionic liquids could be used to control the size of in situ generated ruthenium nanoparticles? *J. Mater. Chem.* **2009**, *19*, 3624−3631.

(4) Zhang, Y.; Gao, H.; Joo, Y.-H.; Shreeve, J. M. Ionic Liquids as Hypergolic Fuels. *Angew. Chem., Int. Ed.* **2011**, *50*, 9554−9562.

(5) Zhang, Y.; Shreeve, J. M. Dicyanoborate-Based Ionic Liquids as Hypergolic Fluids. *Angew. Chem., Int. Ed.* **2011**, *50*, 935−937.

(6) Myasoedova, G. V.; Molochnikova, N. P.; Mokhodoeva, O. B.; Myasoedov, B. F. Application of Ionic Liquids for Solid-Phase Extraction of Trace Elements. *Anal. Sci.* **2008**, *24*, 1351−1353.

(7) He, L.; Tao, G.-H.; Parrish, D. A.; Shreeve, J. M. Nitrocyanamide-Based Ionic Liquids and Their Potential Applications as Hypergolic Fuels. *Chemistry* **2010**, *16*, 5736−5743.

(8) Schneider, S.; Hawkins, T.; Ahmed, Y.; Rosander, M.; Hudgens, L.; Mills, J. Green Bipropellants: Hydrogen-Rich Ionic Liquids that Are Hypergolic with Hydrogen Peroxide. *Angew. Chem., Int. Ed.* **2011**, *50*, 5886−588.

(9) Schneider, S.; Hawkins, T.; Rosander, M.; Vaghjiani, G.; Chambreau, S.; Drake, G. Ionic Liquids as Hypergolic Fuels. *Energy Fuels* **2008**, *22*, 2871−2872.

(10) Costa Gomes, M. F.; Canongia Lopes, J. N.; Padua, A. A. H. Thermodynamics and Micro Heterogeneity of Ionic Liquids. *Top. Curr. Chem.* **2009**, *290*, 161−183.

(11) Wang, Y.; Voth, G. A. Unique Spatial Heterogeneity in Ionic Liquids. *J. Am. Chem. Soc.* **2005**, *127*, 12192−12193.

(12) Shimizu, K.; Costa Gomes, M. F.; Pádua, A. A. H.; Reselo, L. P. N.; Canongia Lopes, J. N. Three commentaries on the nano-segregated structure of ionic liquids. *J. Mol. Struct. THEOCHEM* **2010**, *946*, 70−76.

(13) Shilov, V. V.; Batalin, G. I. Evaluation of the Micro-heterogeneous Structure of Complex Liquids. *J. Strukt. Chem.* **1972**, *13*, 855−856.

(14) Bowers, J.; Butts, C. P.; Martin, P. J.; Vergara-Gutierrez, M. C. Aggregation Behavior of Aqueous Solutions of Ionic Liquids. *Langmuir* **2004**, *20*, 2191−2198.

(15) Ivanova, L. N.; Sultanova, R. M.; Zlotskii, S. S. Effect of Imidazolium Salts on the Catalytic Reaction of 1,3-Dioxolanes with Methyl Diazoacetate. *Russ. J. Gen. Chem.* **2011**, *81*, 106−108.

(16) Stoesser, R.; Herrmann, W.; Zehl, A.; Strehmel, V.; Laschewsky, A. ESR Spin Probes in Ionic Liquids. *ChemPhysChem* **2006**, *7*, 1106−1111.

(17) Strehmel, V.; Laschewsky, A.; Stoesser, R.; Zehl, A.; Herrmann, W. Mobility of spin probes in ionic liquids. *J. Phys. Org. Chem.* **2003**, *19*, 318−325.

(18) Kawai, A.; Hidemori, T.; Shibuy, K. Polarity of Room-Temperature Ionic Liquid as Examined by EPR Spectroscopy. *Chem. Lett.* **2004**, *33*, 1464−1465.

(19) Chumakova, N. A.; Pergushov, V. I.; Vorobiev, A. K.; Kokorin, A. I. Rotational and Translational Mobility of Nitroxide Spin Probes in Ionic Liquids and Molecular Solvents. *Appl. Magn. Reson.* **2010**, *39*, 409−421.

(20) Neve, F.; Francescangeli, O.; Crespini, A. Crystal architecture and mesophase structure of long-chain N-alkylpyridinium tetrachlorometallates. *Inorg. Chim. Acta* **2002**, *338*, 51−58.

(21) Bowlas, C. J.; Bruce, D. W.; Seddon, K. R. Liquid-crystalline ionic liquids. *Chem. Commun.* **1996**, 1625−1626.

(22) Neve, F.; Crispini, A.; Armentano, S.; Francescangeli, O. Synthesis, Structure, and Thermotropic Mesomorphism of Layered N-Alkylpyridinium Tetrahalopalladate(II) Salts. *Chem. Mater.* **1998**, *10*, 1904−1913.

(23) Del Sesto, R. E.; McCleskey, T. M.; Burrell, A. K.; Baker, G. A.; Thompson, J. D.; Scott, B. L.; Wilkes, J. S.; Williams, P. Structure and magnetic behavior of transition metal based ionic liquids. *Chem. Commun.* **2008**, 447−449.

(24) Neve, F.; Impéror-Clerc, M. An Ia$\bar{3}$d thermotropic cubic phase from N-alkylpyridinium tetrahalocuprates. *Liquid Cryst.* **2004**, *31*, 907−912.

(25) Zhang, P.; Gong, Y.; Lv, Y.; Guo, Y.; Wang, Y.; Wang, C.; Li, H. Ionic liquids with metal chelate anions. *Chem. Commun.* **2012**, *48*, 2334−2336.

(26) Lin, S.; W. Liu, W.; Li, Y.; Wu, Q.; Wang, E.; Zhan, Z. Preparation of polyoxometalates in ionic liquids by ionothermal synthesis. *Dalton Trans.* **2010**, *39*, 174−1744.

(27) Pakhomova, A. S.; Krivovichev, S. V. Ionothermal synthesis and characterization of alkalimetal polyoxometallates: Structural trends in the $(emim)_m[A_n(Mo_8O_{26})]$ (emim=1-ethyl-3-methylimidazolium; m=2,3; n=1,2; A=K, Rb, Cs) group of compounds. *Inorg. Chem. Commun.* **2010**, *13*, 1463−1465.

(28) Lee, C. K.; Peng, H. H.; Lin, I. J. B. Liquid Crystals of N,N′-Dialkylimidazolium Salts Comprising Palladium(II) and Copper(II) Ions. *Chem. Mater.* **2004**, *16*, 530−536.

(29) Taubert, A. Heavy Elements in Ionic Liquids. *Top. Curr. Chem.* **2009**, *290*, 127−159.

(30) Gamlen, G. A.; Jordan, D. O. A Spectrophotometric Study of the Iron(III) Chloro-complexes. *J. Chem. Soc.* **1953**, 1435−1443.

(31) Brealey, G. J.; Uri, N. Photochemical OxidationReduction and Photocatalysis. The Photochemical Activity of $FeCl_4^-$ in Alcohol as Oxidizing Agent and as Catalyst. *J. Chem. Phys.* **1952**, *20*, 257−262.

(32) Wertz, D. L.; Kruh, R. F. Structure of Iron (III) Chloride−Methanol Solutions. *J. Chem. Phys.* **1969**, *50*, 4013−4018.

(33) Katzin, L. I. Ionization Differences Between Coordination States of a Cation. Octahedral-Tetrahedral Equilibrium of TransitionElement Chlorides in Dimethylformamide. *J. Chem. Phys.* **1962**, *36*, 3034−3041.

(34) McCusker, P. A.; Scholastica Kennard, S. M. A Spectrophotometric Study of Anhydrous Iron(III) Chloride and Tetrachloroferric (III) Acid in Dioxane and Other Ethers. *J. Am. Chem. Soc.* **1959**, *81*, 2976−2982.

(35) Friedman, H. L. The Visible and Ultraviolet Absorption Spectrum of the Tetrachloroferrate(III) Ion in Various Media. *J. Am. Chem. Soc.* **1952**, *74*, 5−10.

(36) Bjerrum, J.; Lukes, I. The Iron(III)-Chloride System. A Study of the Stability Constants and of the Distribution of the Tetrachloro Species between Organic Solvents and Aqueous Chloride Solutions. *Acta Chem. Scand. A* **1986**, *40*, 31−40.

(37) Witten, E. H.; Reiff, W. M.; Lazar, K.; Sullivan, B. W.; Foxman, B. M. The Ferric Chloride-a-Diamine System. 3. X-ray Crystallographic, Magnetic Susceptibility, and Zero- and High-Field Mössbauer Spectroscopy Investigation of $[Fe(2,2'\text{-bpy})_2Cl_2][FeC1_4]$: Slow Paramagnetic Relaxation and Magnetic Ordering of Complex Bimetallic Salts. *Inorg. Chem.* **1985**, *24*, 4585−4591.

(38) Woodward, L. A.; Taylor, M. J. Raman Effect and Solvent Extraction. Part II. Spectra of the Tetrachloroindate and Tetrachloroferrate Ions. *J. Chem. Soc.* **1960**, 4473−4477.

(39) Myers, R. J.; Metzler, D. E. The Distribution of Ferric Iron between Hydrochloric Acid and Isopropyl Ether Solutions. II. Polymerization of the Iron in the Ether Phase, the Effect of the

Acid Concentration on the Distribution, and the Two-Ether-Phase Region. *J. Am. Chem. Soc.* **1950**, *72*, 3772−3776.
(40) Weiner, H.; Lunk, H.-J.; Stösser, R.; Lück, R. Synthese, Charakterisierung und EPR-spektroskopische Untersuchung von Heteropolyverbindungen mit tetraedrisch bzw. oktaedrisch koordiniertem Eisen(III). *Z. Allgem. Anorg. Chem.* **1989**, *572*, 164−174.
(41) Scholz, G.; Stösser, R.; Krossner, M.; Klein, J. Modelling of Multifrequency ESR Spectra of Fe^{3+} Ions in Crystalline and Amorphous Materials: A Simplified Approach to Determine Statistical Distributions of Spin-Spin Coupling Parameters. *Appl. Magn. Reson.* **2001**, *21*, 105−123.
(42) Buzaré, J. Y.; Silly, G.; Klein, J.; Scholz, G.; Stösser, R.; Nofz, M. Electron paramagnetic resonance investigations of α-Al_2O_3 powders doped with Fe^{3+} ions: experiments and simulations. *J. Phys.: Condens. Matter* **2002**, *14*, 10331−10348.
(43) Stoesser, R.; Herrmann, W.; Zehl, A.; Laschewsky, A.; Strehmel, V. Microviscosity and Micropolarity Effects of Imidazolium Based Ionic Liquids Investigated by Spin Probes Their Diffusion and Spin Exchange. *Z. Phys. Chem.* **2006**, *220*, 1309−1342.
(44) Weil, J. A.; Bolton, J. R. *Electron paramagnetic resonance: elementary theory and practical applications*; John Wiley & Sons: Hoboken, 2007.
(45) Eaton, G. R.; Eaton, S. S.; Barr, D. P.; Weber, R. T. *Quantitative EPR*; Springer: New York, 2010.
(46) Stößer, R.; Feist, M.; Patzwaldt, K.; Menzel, M.; Emmerling, F. Redox reactions of $K_3[Fe(CN)_6]$ during mechanochemically stimulated phase transitions of AlOOH. *J. Phys. Chem. Solids* **2011**, *72*, 794−799.
(47) Hertel, G. R.; Clark, H. M. Paramagnetic Resonance Behaviour of Tetrachloroferrate Ion in Isopropyl Ether. *J. Phys. Chem.* **1961**, *65*, 1930−1932.
(48) Stösser, R.; Nofz, M. ESR Spectroscopy on Glasses and Glassy-Crystalline Materials - New Opportunities for Material Scientists. *Glastech. Ber. Glass Sci. Technol.* **1994**, *67*, 156−170.
(49) Nistor, S. V.; Velter Stefanescu, M. Interstitial cubic Fe^{3+} centres in NaCl crystals. *J. Phys. C: Solid State Phys.* **1985**, *18*, 397−401.
(50) Rudowicz, C. Transformation relations for the conventional O_k^q and normalised $O_k'^q$ Stevens operator equivalents with k = 1 to 6 and $-k \leq q \leq k$. *J. Phys. C: Solid State Phys.* **1985**, *18*, 1415−1430.
(51) Grampp, G.; Kattnig, D.; Mladenova, B. ESR-spectroscopy in ionic liquids: Dynamic linebroadening effects caused by electron-self exchange reactions within the methylviologene redox couple. *Spectrochim. Acta A* **2006**, *63*, 821−825.
(52) Hayes, R.; Imberti, S.; Warr, G. G.; Atkin, R. How Water Dissolves in Protic Ionic Liquids. *Angew. Chem.* **2012**, *124*, 7586−7589.
(53) Weber, C. C.; Masters, A. F.; Maschmeyer, T. Pseudo-Encapsulation—Nanodomains for Enhanced Reactivity in Ionic Liquids. *Angew. Chem., Int. Ed.* **2012**, *51*, 11483−11486.
(54) Wang, Y.; Voth, G. A. Unique Spatial Heterogeneity in Ionic Liquids. *J. Am. Chem. Soc.* **2005**, *127*, 12192−12193.
(55) Costa Gomes, M. F.; Canongia Lopes, J. N.; Padua, A. A. H. Thermodynamics and Micro Heterogeneity of Ionic Liquids. *Top. Curr. Chem.* **2009**, *290*, 161−183.
(56) Shimizu, K.; Costa Gomes, M. F.; Padua, A. A. H.; Rebelo, L. P. N.; Canongia Lopes, J. N. Three commentaries on the nano-segregated structure of ionic liquids. *J. Mol. Struct. THEOCHEM* **2010**, *946*, 70−76.
(57) Shi, C.; Zhao, Y.; Xin, J.; Wang, J.; Lu, X.; Zhang, X.; Zhang, S. Effects of cations and anions of ionic liquids on the production of 5-hydroxymethylfurfural from fructose. *Chem. Comm.* **2012**, *48*, 4103−4105.
(58) Lexa, D.; Momenteau, M.; Mispelter, J. Characterization of the Reduction Steps of Fe(III) Porphyrins. *Biochim. Biophys. Acta* **1974**, *338*, 151−163.
(59) Skrzypek, D.; Madejska, I.; Habdas, J. The electronic and magnetic properties of iron(III) derivatives of selected substituted meso-tetraphenyl porphyrins: ESR spectroscopic study. *J. Phys. Chem. Solids* **2005**, *66*, 91−97.